ChemComm

COMMUNICATION

View Article Online
View Journal | View Issue

Cite this: *Chem. Commun.*, 2023, **59**, 7048

Received 2nd November 2022,
Accepted 10th May 2023

DOI: 10.1039/d2cc05930d

rsc.li/chemcomm

Long-term imaging of intranuclear Mg^{2+} dynamics during mitosis using a localized fluorescent probe†

Yusuke Matsui,‡[a] Toshiyuki Kowada,‡[bc] Yi Ding,[c] Priya Ranjan Sahoo,[b] Kazuya Kikuchi *[ad] and Shin Mizukami *[bc]

A novel fluorescent Mg^{2+} probe was developed based on a small molecule–protein hybrid. This probe enables subcellular targeting, long-term imaging, and high selectivity for Mg^{2+} over Ca^{2+}. Using ratiometric fluorescence microscopy with a co-localized standard fluorophore, the variations in intranuclear Mg^{2+} concentrations during mitosis could be visualized.

The magnesium ion (Mg^{2+}) is an essential divalent cation involved in various cellular functions.[1–3] For cellular homeostasis, intracellular Mg^{2+} concentration ($[Mg^{2+}]_i$) is maintained in the range of 0.5–1 mM by influx and efflux through Mg^{2+} channels and transporters and buffering by ATP.[4,5] Although $[Mg^{2+}]_i$ changes during physiological processes,[2,3,6,7] subcellular Mg^{2+} dynamics have not been extensively investigated. We have demonstrated a protein labeling technology is a valuable method to localize synthetic fluorescent probes for investigating subcellular ion concentrations.[6,8–10] For Mg^{2+} imaging, we developed an organelle-targetable Mg^{2+} probe, MGH, with a chloroalkyl HaloTag ligand and demonstrated its long-term retention in HaloTag-expressing cells.[6] HaloTag can be genetically expressed in subcellular regions by appending a localization peptide sequence, and functional compounds with a HaloTag ligand can be specifically targeted to the site.[11] MGH adopted *o*-aminophenol-*N*,*N*,*O*-triacetic acid (APTRA) as the Mg^{2+} chelator. Although APTRA can recognize intracellular Mg^{2+} with appropriate affinity ($K_{d,Mg}$ = 1–4.7 mM), it also shows strong affinity for Ca^{2+} ($K_{d,Ca}$ = 6–35 μM).[12] This low Mg^{2+} selectivity of APTRA-based probes requires the simultaneous imaging of Mg^{2+} and Ca^{2+} dynamics in living cells to confirm if the fluorescence responses of the Mg^{2+} probes are caused by the change in $[Mg^{2+}]$ or $[Ca^{2+}]$. Furthermore, Ca^{2+} is present at more than hundreds of μM in some organelles, such as the mitochondria, endoplasmic reticulum (ER), and Golgi apparatus.[13] Therefore, APTRA-based organelle-targetable probes[6,14,15] have not yet been used to precisely detect Mg^{2+} dynamics in local subcellular regions.

KMG-104-AsH is a Mg^{2+} probe that enables subcellular localization by utilizing a tetracysteine peptide tag (TC-tag).[16] However, the cellular toxicity of ethanedithiol used to suppress non-specific signals in the TC-tag technology hampers long-term imaging for more than 4 h.[17] Therefore, there is a need to develop novel fluorescent probes that exhibit high Mg^{2+} selectivity and organelle targetability. In this study, we developed a novel fluorescent Mg^{2+} probe, MGQ-2H (Fig. 1a), which can be localized to the subcellular target regions and used to visualize long-term local Mg^{2+} dynamics with little interference by Ca^{2+}. These remarkable properties of MGQ-2H enabled us to monitor nuclear Mg^{2+} fluctuations during mitosis.

Previously, we reported a Mg^{2+} chelator, 2,8-dicarboxyquinoline (DCQ), with superior selectivity for Mg^{2+} over Ca^{2+} and the Mg-ATP complex and developed DCQ-based fluorescent probes.[18,19] MGQ-2H consists of a fluorescent Mg^{2+} probe (MGQ-2) and a HaloTag ligand for specific and long-term subcellular targeting (Fig. 1b). MGQ-2H was synthesized from the methyl ester form of MGQ-2 according to Schemes S1 and S2 (ESI†). Then, one phenoxy and two carboxy groups of MGQ-2H were protected with an acetoxymethyl (AM) ester group to yield the cell membrane-permeable form, MGQ-2H(AM), for live-cell imaging. Since AM groups are spontaneously hydrolyzed by intracellular esterases,[17] MGQ-2H(AM) was designed to convert into the Mg^{2+}-coordinating form in living cells.

While the absorption spectra of MGQ-2H showed only slight variations upon the addition of Mg^{2+}, the fluorescence intensity

[a] *Graduate School of Engineering, Osaka University, Suita, Osaka 565-0871, Japan. E-mail: kkikuchi@mls.eng.osaka-u.ac.jp*
[b] *Institute of Multidisciplinary Research for Advanced Materials, Tohoku University, Sendai, Miyagi 980-8577, Japan. E-mail: shin.mizukami@tohoku.ac.jp*
[c] *Graduate School of Life Sciences, Tohoku University, Sendai, Miyagi 980-8577, Japan*
[d] *WPI-Immunology Frontier Research Center, Osaka University, Suita, Osaka 565-0871, Japan*

† Electronic supplementary information (ESI) available. See DOI: https://doi.org/10.1039/d2cc05930d

‡ Y. M. and T. K. contributed equally to this work.

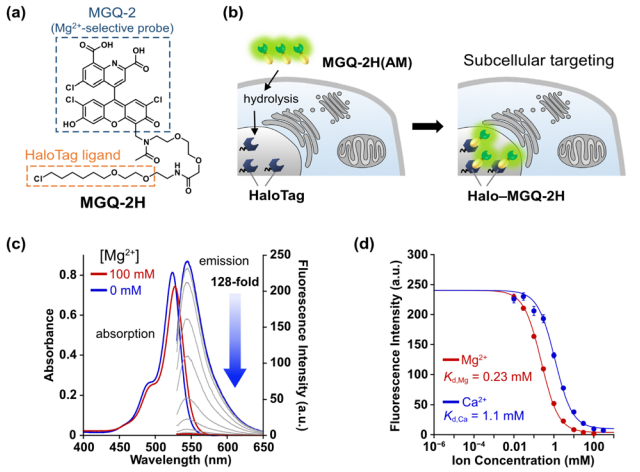

Fig. 1 (a) Chemical structure of MGQ-2H. (b) Schematic illustration of the subcellular targeting of MGQ-2H using HaloTag technology. (c) Absorption and emission (λ_{ex} = 524 nm) spectra of MGQ-2H (10 μM for absorption, 1 μM for emission) in 100 mM HEPES buffer (pH 7.4) containing 115 mM KCl, 20 mM NaCl, and different concentrations of Mg^{2+} at 37 °C. (d) Mg^{2+}- and Ca^{2+}-titration curves of MGQ-2H emission (λ_{ex} = 524 nm, λ_{em} = 545 nm). Error bars denote the standard deviation (SD) (n = 3).

decreased considerably depending on the $[Mg^{2+}]$ (Φ_{free} = 0.44, Φ_{bound} < 0.01) (Fig. 1c and Table S1, ESI†). This turn-off fluorescence response is attributed to donor-excited photo-induced electron transfer (d-PeT) as reported in MGQ-2.[18] The apparent dissociation constants of MGQ-2H for Mg^{2+} ($K_{d,Mg}$) and Ca^{2+} ($K_{d,Ca}$) were determined to be 0.23 and 1.1 mM, respectively (Fig. 1d and Table S1, ESI†). The detection limit of MGQ-2H for Mg^{2+} was also determined to be 0.028 mM (Fig. S1, ESI†). The effect of Ca^{2+} was also estimated by varying the $[Ca^{2+}]$ with the physiological $[Mg^{2+}]$ (0.5 mM). The presence of Ca^{2+} up to 100 μM had no noticeable effect on the fluorescence of MGQ-2H, whereas 1 mM Ca^{2+} caused a 21% decrease in fluorescence (Fig. S2, ESI†). We then examined the metal-ion selectivity of MGQ-2H, resulting in a decrease in fluorescence in the presence of 1 μM of transition metal ions (Fe^{2+}, Co^{2+}, Ni^{2+}, Cu^{2+}, and Zn^{2+}). Furthermore, the K_d values of MGQ-2H for these transition metal ions were investigated (Fig. S3, ESI†). The pH responsiveness of MGQ-2H was measured at free and fully Mg^{2+}-bound states (Fig. S4, ESI†). MGQ-2H barely responded to pH changes in the neutral pH range. On the other hand, the fluorescence intensity decreased in the acidic pH region, indicating that protonation of the quinoline moiety induced d-PeT-based fluorescence quenching. The similar physical properties of MGQ-2 (Table S1, ESI†) indicate that the introduction of the HaloTag ligand barely affected the optical and coordination properties of MGQ-2H.

The HaloTag-conjugated MGQ-2H (Halo–MGQ-2H) showed almost the same Mg^{2+}-dependent spectral changes for absorption and emission as MGQ-2H (Fig. S5a and b, ESI†). However, the K_d values for Mg^{2+} and Ca^{2+} were slightly decreased to 0.13 and 0.65 mM, respectively (Fig. S5c and Table S1, ESI†), corresponding to the tendency of the previously reported HaloTag-conjugated Mg^{2+} probe.[6] Nevertheless, these properties are considered suitable in most intracellular regions for the imaging of intracellular Mg^{2+} dynamics without interference from Ca^{2+}, with the exception of the Golgi and ER that possess a concentration of greater than 100 μM Ca^{2+}.[13]

Next, we examined the subcellular targeting property of MGQ-2H in HEK293 cells. Probe fluorescence was observed over the entire region of non-transfected cells incubated with MGQ-2H(AM) (Fig. S6, ESI†). This result indicates that the anionic carboxylates of the enzymatically hydrolyzed probes reduced the membrane permeability, resulting in the longer residence time in living cells. Additionally, the fluorescence intensity of MGQ-2H appeared higher in the nucleus than in the cytoplasm (Fig. S7, ESI†). Since a similar phenomenon was observed in the case of Magnesium Green (Fig. S7b, ESI†), $[Mg^{2+}]$ in the nucleus ($[Mg^{2+}]_{nuc}$) may be slightly higher than in the cytoplasm, or Mg^{2+} probes may tend to accumulate in the nucleus, although the reason is unclear. Next, to localize MGQ-2H to subcellular regions, HEK293 cells were transfected with plasmids encoding HaloTag (for cytoplasm and nucleus), Halo-NLS (for nucleus), or Lyn_{11}-Halo (for the inner leaflet of the plasma membrane). The fluorescence microscopy images indicated that MGQ-2H was successfully localized to the target subcellular compartments.

To examine the fluorescence response of Halo–MGQ-2H upon variation in $[Mg^{2+}]_i$, a FLAG-tagged Mg^{2+} transporter, ancient conserved domain protein/cyclin M4 (CNNM4),[20] was transiently expressed in HEK293 cells stably expressing Halo-EGFP (Fig. S8, ESI†), and the cells were incubated with MGQ-2H(AM) in 40 mM Mg^{2+} buffer. The extracellular solution was then replaced with a Mg^{2+}-free buffer to release intracellular Mg^{2+} *via* CNNM4. To minimize the fluorescence changes caused by the cell morphological changes and the focal drift, we used the fluorescence ratiometry of MGQ-2H over EGFP to analyze $[Mg^{2+}]_i$ fluctuations (Fig. 2b and Fig. S9, ESI†). After Mg^{2+} depletion from the extracellular solution, the fluorescence ratio immediately increased, although CNNM4 non-expressing cells showed a lower increase in fluorescence (Fig. 2a and b). These results indicate that Halo–MGQ-2H functions as a fluorescent probe for the real-time monitoring of Mg^{2+} in living cells.

We also investigated the unresponsiveness of Halo–MGQ-2H toward Ca^{2+} influx in living cells. HEK293 cells expressing HaloTag and a Ca^{2+} indicator, R-GECO,[21] were loaded with MGQ-2H(AM) or an APTRA-based Mg^{2+} probe, Magnesium Green(AM). After adding ionomycin to induce a Ca^{2+} influx, R-GECO quickly showed a significant increase in fluorescence, indicating an increase in $[Ca^{2+}]_i$ (Fig. 2c and d). Similarly, Magnesium Green exhibited the fluorescence increase in response to Ca^{2+} influx, indicating false-positive fluorescence responses due to the low selectivity toward Mg^{2+} over Ca^{2+}. In contrast, Halo–MGQ-2H showed no fluorescence decrease upon adding ionomycin, indicating no response to influxed Ca^{2+} (Fig. 2d). However, the fluorescence gradually increased 1.2–1.8-fold in 5 min (Fig. S10, ESI†), which might be attributed to the efflux of metal ions, including Mg^{2+} and Fe^{2+}, to compensate for the variation in the Ca^{2+}-influx-induced membrane potential.[22–25] These results indicate that MGQ-2H enabled the exclusive detection of changes in

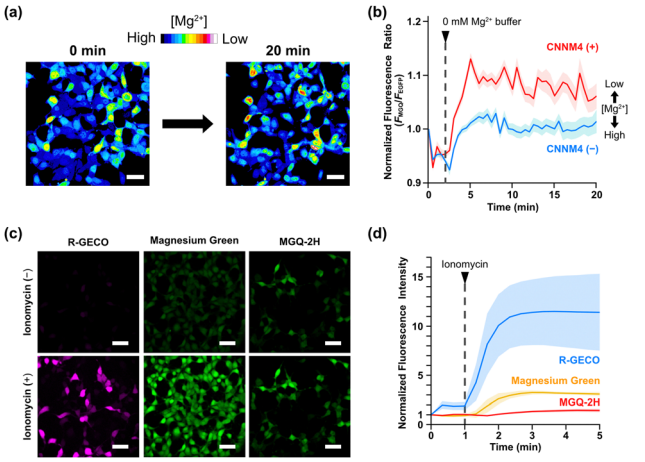

Fig. 2 (a) and (b) Confocal fluorescence microscopic images of Halo–MGQ-2H (a) and normalized fluorescence ratio of Halo–MGQ-2H over Halo-EGFP (b) in HEK293 cells expressing Halo-EGFP and CNNM4-FLAG (n = 24 cells, 3 experiments). Scale bar: 40 μm. (c) Ca^{2+} responsivity of Halo–MGQ-2H in HEK293 cells. Scale bar: 80 μm. (d) Normalized fluorescence intensity of R-GECO, Magnesium Green, and Halo–MGQ-2H in HEK293 cells. Ionomycin was added at 1 min (n = 10 cells). The solid lines and shaded area indicate mean and SEM (b) or SD (d), respectively.

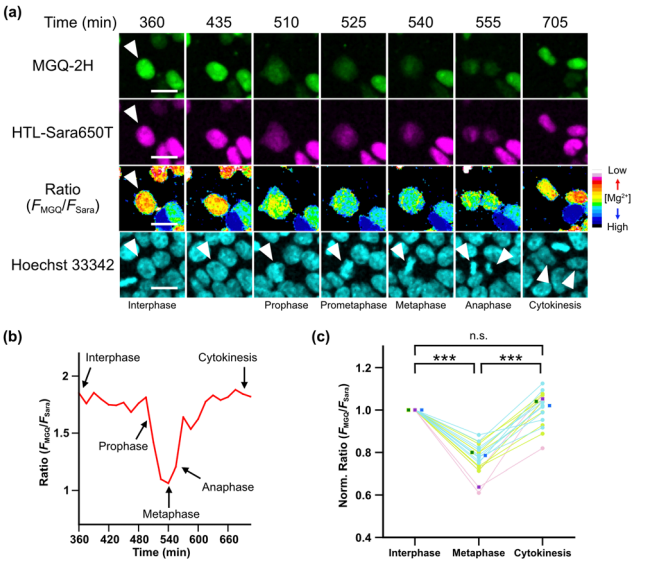

Fig. 3 (a) Confocal fluorescence imaging of intranuclear Mg^{2+} dynamics in HEK293T cells during mitosis. Scale bar: 20 μm. (b) Time course of fluorescence ratio (MGQ-2H/HTL-Sara650T) of a mitotic cell indicated by an arrowhead in (a). (c) Quantitative analysis of the ratio during each stage of mitosis. A circular dot indicates each data point, and a rectangle dot indicates the median of each experiment (n = 19 cells, 3 experiments). ***$p < 0.001$. n.s.: not significant (p = 0.61).

$[Mg^{2+}]_i$ without responding to Ca^{2+} fluctuations, although care must be taken in interpreting the intracellular ion fluxes resulting from the cellular response.

We performed long-term Mg^{2+} imaging in living cells. Mg^{2+} plays a critical role in chromatin condensation by weakening the electrostatic repulsion of negatively-charged chromatin.[26–29] The correlation between $[Mg^{2+}]_{nuc}$ and chromatin morphology during mitosis is of significant interest. However, the extracellular leakage and lack of subcellular targetability of small molecule-based Mg^{2+} probes have hampered the long-term imaging of intracellular Mg^{2+} dynamics. Although MGQ-2 lacking a targeting ligand showed prompt extracellular leakage, the fluorescence of MGQ-2H was continuously observed for 24 h in the nucleus of HEK293T cells expressing Halo-NLS, without significant variations in the fluorescence intensity (Fig. S11, ESI†). Because mitosis takes place over several hours, we applied the long-term intracellular retention property of MGQ-2H for imaging intranuclear Mg^{2+} dynamics during mitosis.

For quantitative imaging, we calculated the fluorescence ratio of MGQ-2H and the internal standard (F_{MGQ}/F_{Sara}), Si-rhodamine dye (HTL-Sara650T) (Fig. S12, ESI†). Such a ratiometric method using a conjugatable standard fluorophore excludes the influence of subcellular concentration differences.[6,8–10] HEK293T cells expressing Halo-NLS were incubated with MGQ-2H(AM) and subsequently with HTL-Sara650T, followed by time-lapse imaging for 24 h. Similar to the case for the non-transfected cells in Fig. S6 (ESI†), the fluorescence signals of free MGQ-2H were observed in some cells at early time points. However, the fluorescence signals of free MGQ-2H reached a negligible level at 45 min (Fig. S13, ESI†). In mitotic cells, chromosome condensation started at 510 min (prophase) and progressed at 525 min (prometaphase) (Fig. 3a and Movie S1, ESI†). The chromosome aligned at the equatorial plane at 540 min (metaphase), the nucleus divided into two nuclei at 555 min (anaphase), and cytokinesis was completed at 705 min. During mitosis, F_{Sara} appeared to decrease, probably due to fluorophore dilution caused by the nuclear envelope fragmentation and nuclear protein diffusion throughout the cells. While the F_{MGQ}/F_{Sara} did not show remarkable changes during interphase, it significantly decreased from that in prophase and had the minimum value during metaphase. The ratio then increased from anaphase and returned to its initial level within 60 min (Fig. 3b). Cytokinesis was observed after the F_{MGQ}/F_{Sara} became almost constant. We evaluated the differences in the F_{MGQ}/F_{Sara} of 19 cells during interphase, metaphase, and cytokinesis, resulting in that the F_{MGQ}/F_{Sara} values in metaphase were significantly lower than those in interphase and cytokinesis (Fig. 3c and Fig. S14 and Table S2, ESI†).

Since the low ratio value corresponds to high $[Mg^{2+}]$, these results indicate that $[Mg^{2+}]_{nuc}$ increased from prophase, showed the highest value at metaphase, then decreased from anaphase, and returned to the initial level before cytokinesis, suggesting the correlation between $[Mg^{2+}]_{nuc}$ and chromatin condensation level. This variation in $[Mg^{2+}]_i$ during mitosis is consistent with a previous report using a fluorescent protein-based Mg^{2+} probe, MARIO,[26] and supports the reliability of the Halo–MGQ-2H system. Considering the physiological range of $[Mg^{2+}]_i$ (0.5–1 mM), the stronger affinity of Halo–MGQ-2H ($K_{d,Mg}$ = 0.13 mM) over MARIO ($K_{d,Mg}$ = 7.2 mM) indicates the potential of our probe for various cellular applications.

To verify if the F_{MGQ}/F_{Sara} changes during mitosis were due to $[Mg^{2+}]_{nuc}$ fluctuation, we further examined the probe photobleaching and the effects of other metal ions. The fluorescence signals of

Halo–MGQ-2H in non-mitotic cells were near constant for more than 20 h (Fig. S15, ESI†), indicating that the photobleaching was almost negligible during the long-term imaging. Fig. S2 and S3 (ESI†) indicates that Zn^{2+}, Cu^{2+}, and Fe^{2+} potentially affect the imaging results. However, physiological concentrations of Zn^{2+} and Cu^{2+} are reported to be sub-nanomolar and femto–attomolar,[30] respectively. We also confirmed that Halo–MGQ-2H did not exhibit a significant fluorescence change upon elevation of intracellular Zn^{2+} concentration ($[Zn^{2+}]_i$) by adding zinc pyrithione (ZPT) (Fig. S16, ESI†). The $[Zn^{2+}]_i$ change upon ZPT addition was also confirmed by monitoring the fluorescence increase of a HaloTag-conjugated fluorescent Zn^{2+} probe.[10] Regarding Fe^{2+}, the most of iron ions (Fe^{2+}/Fe^{3+}) are present as the protein-bound states, and 0.2–0.5 μM of the labile irons are present in cells.[30] Hence, fluctuations in intracellular Fe^{2+} could potentially affect the imaging results of MGQ-2H. Since there are no reports on the change in $[Fe^{2+}]$ during mitosis, Fe^{2+}-selective imaging should be performed. While this possibility should be considered, the other data suggest that Halo–MGQ-2H fluorescence variation during mitosis mainly reflected the $[Mg^{2+}]_{nuc}$ fluctuations.

In conclusion, we developed a novel fluorescent Mg^{2+} probe, MGQ-2H, which exclusively labels HaloTags expressed in cells. MGQ-2H showed suitable affinity for detecting changes in $[Mg^{2+}]_i$ and very weak affinity for Ca^{2+} to monitor long-term Mg^{2+} dynamics in the cytosol and nucleus. Owing to these remarkable properties, MGQ-2H was used for Mg^{2+} imaging during mitosis. Ratiometric imaging using MGQ-2H and HTL-Sara650T successfully visualized the increase in $[Mg^{2+}]_{nuc}$ from prophase to metaphase and subsequent decrease from anaphase to cytokinesis. The physical properties of MGQ-2H and live-cell imaging data indicate that MGQ-2H is very useful for analyzing the long-term dynamics of intracellular Mg^{2+} without any interference by probe leakage and $[Ca^{2+}]_i$ fluctuations in the cytosol and nucleus. However, considering fluorescence quenching in acidic solutions and relatively high affinity for Fe^{2+} and Zn^{2+}, fluorescence signal changes should be carefully interpreted in the biological applications in which fluctuations in transition metal concentrations or acidification occur. In addition, the Mg^{2+}-dependent quenching property of MGQ-2H is not beneficial for intuitive analysis and needs to be improved in the future. Nevertheless, since APTRA-based Mg^{2+} probes are not suitable for the detailed analysis of intracellular Mg^{2+} dynamics in some cases where Ca^{2+} fluctuation simultaneously occurs, for example, by TRPM7,[31] our new probe can aid in elucidating unknown intracellular Mg^{2+} dynamics.

This research was supported by JSPS KAKENHI (No. JP18 H02102, JP21H05252, JP21H04706), the Takeda Science Foundation, the Tokyo Biochemical Research Foundation, AMED-CREST (21gm1410006h0001), and the ''Dynamic Alliance for Open Innovation Bridging Human, Environment and Materials'' Research Program in the ''Network Joint Research Center for Materials and Devices''. We thank Y. Funato and H. Miki (Osaka University) for their helpful discussion and for providing the *CNNM4* gene and HEK293 cells.

Conflicts of interest

There are no conflicts to declare.

Notes and references

1 A. Hartwig, *Mutat. Res.*, 2001, **475**, 113–121.
2 F. Y. Li, B. Chaigne-Delalande, C. Kanellopoulou, J. C. Davis, H. F. Matthews, D. C. Douek, J. I. Cohen, G. Uzel, H. C. Su and M. J. Lenardo, *Nature*, 2011, **475**, 471–476.
3 F. I. Wolf and V. Trapani, *Clin. Sci.*, 2008, **114**, 27–35.
4 A. M. P. Romani, *Arch. Biochem. Biophys.*, 2011, **512**, 1–23.
5 R. D. Grubbs, *Biometals*, 2002, **15**, 251–259.
6 Y. Matsui, Y. Funato, H. Imamura, H. Miki, S. Mizukami and K. Kikuchi, *Chem. Sci.*, 2017, **8**, 8255–8264.
7 K. A. Feeney, L. L. Hansen, M. Putker, C. Olivares-Yañez, J. Day, L. J. Eades, L. F. Larrondo, N. P. Hoyle, J. S. O'Neill and G. Van Ooijen, *Nature*, 2016, **532**, 375–379.
8 T. Kowada, T. Watanabe, Y. Amagai, R. Liu, M. Yamada, H. Takahashi, T. Matsui, K. Inaba and S. Mizukami, *Cell Chem. Biol.*, 2020, **27**, 1521–1531.
9 T. Kowada, T. Watanabe, R. Liu and S. Mizukami, *STAR Protoc.*, 2021, **2**, 100395.
10 R. Liu, T. Kowada, Y. Du, Y. Amagai, T. Matsui, K. Inaba and S. Mizukami, *ACS Sens.*, 2022, **7**, 748–757.
11 G. V. Los, L. P. Encell, M. G. Mcdougall, D. D. Hartzell, N. Karassina, D. Simpson, J. Mendez, K. Zimmerman, P. Otto, G. Vidugiris, J. Zhu, A. Darzins, D. H. Klaubert, R. F. Bulleit and K. V. Wood, *ACS Chem. Biol.*, 2008, **3**, 373–382.
12 R. P. Haugland, *Handbook of Fluorescent Probes and Research Products*, Molecular Probes Inc., Eugene, Oregon, 9th edn, 2002.
13 J. Suzuki, K. Kanemaru and M. Iino, *Biophys. J.*, 2016, **111**, 1119–1131.
14 G. Zhang, J. J. Gruskos, M. S. Afzal and D. Buccella, *Chem. Sci.*, 2015, **6**, 6841–6846.
15 J. J. Gruskos, G. Zhang and D. Buccella, *J. Am. Chem. Soc.*, 2016, **138**, 14639–14649.
16 T. Fujii, Y. Shindo, K. Hotta, D. Citterio, S. Nishiyama, K. Suzuki and K. Oka, *J. Am. Chem. Soc.*, 2014, **136**, 2374–2381.
17 B. A. Griffin, S. R. Adams and R. Y. Tsien, *Science*, 1998, **281**, 269–272.
18 Y. Matsui, K. K. Sadhu, S. Mizukami and K. Kikuchi, *Chem. Commun.*, 2017, **53**, 10644–10647.
19 Y. Matsui, S. Mizukami and K. Kikuchi, *Chem. Lett.*, 2018, **47**, 23–26.
20 D. Yamazaki, Y. Funato, J. Miura, S. Sato, S. Toyosawa, K. Furutani, Y. Kurachi, Y. Omori, T. Furukawa, T. Tsuda, S. Kuwabata, S. Mizukami, K. Kikuchi and H. Miki, *PLoS Genet.*, 2013, **9**, e1003983.
21 Y. Zhao, S. Araki, J. Wu, T. Teramoto, Y.-F. Chang, M. Nakano, A. S. Abdelfattah, M. Fujiwara, T. Ishihara, T. Nagai and R. E. Campbell, *Science*, 2011, **333**, 1888–1891.
22 L. H. Brent, B. Rubenstein, Q. H. Gong and S. J. Wieland, *J. Cell. Physiol.*, 1996, **168**, 155–165.
23 T. Alatossava, H. Jütte, A. Kuhn and E. Kellenberger, *J. Bacteriol.*, 1985, **162**, 413–419.
24 M. Kolisek, P. Launay, A. Beck, G. Sponder, N. Serafini, M. Brenkus, E. M. Froschauer, H. Martens, A. Fleig and M. Schweigel, *J. Biol. Chem.*, 2008, **283**, 16235–16247.
25 C. N. Deshpande, T. A. Ruwe, A. Shawki, V. Xin, K. R. Vieth, E. V. Valore, B. Qiao, T. Ganz, E. Nemeth, B. Mackenzie and M. Jormakka, *Nat. Commun.*, 2018, **9**, 3075.
26 K. Maeshima, T. Matsuda, Y. Shindo, H. Imamura, S. Tamura, R. Imai, S. Kawakami, R. Nagashima, T. Soga, H. Noji, K. Oka and T. Nagai, *Curr. Biol.*, 2018, **28**, 444–451.
27 A. Visvanathan, K. Ahmed, L. Even-Faitelson, D. Lleres, D. P. Bazett-Jones and A. I. Lamond, *PLoS One*, 2013, **8**, e67689.
28 D. F. Hudson, P. Vagnarelli, R. Gassmann and W. C. Earnshaw, *Dev. Cell*, 2003, **5**, 323–336.
29 M. P. F. Marsden and U. K. Laemmli, *Cell*, 1979, **17**, 849–858.
30 T. Dudev and C. Lim, *Chem. Rev.*, 2014, **114**, 538–556.
31 Z.-G. Zou, F. J. Rios, A. C. Montezano and R. M. Touyz, *Int. J. Mol. Sci.*, 2019, **20**, 1877.